Strain path's influence on the elastic behaviour of the TRIP 700 steel

J. Mendiguren [a,*], F. Cortés [b], L. Galdos [a], S. Berveiller [c]

[a] Manufacturing Department, Mondragon University, Loramendi 4, 20500 Arrasate-Mondragon, Spain
[b] DeustoTech–Deusto Institute of Technology, Faculty of Engineering, University of Deusto, Avenida de las Universidades 24, 48007 Bilbao, Spain
[c] Laboratoire d'Étude des Microstructures et de Mécanique des Matériaux, LEM3, UMR CNRS 7239, Arts et Métiers ParisTech, 4 rue Augustin Fresnel, 57078 Metz Cedex 03, France

A B S T R A C T

This paper deals with the analysis of the strain path's influence on the elastic behaviour of TRIP 700 steel; it aims to validate the cyclic testing method to characterise inelastic behaviour of advanced high strength steels (AHSS). Different cyclic tests are done, where the strain path is changed from test to test. Large deformation strain gages are used to determine the inelastic behaviour of the specimens at macro-level. At a lower scale, stress measurements are carried out using the XRD technique during an in-situ tensile test: ferrite and austenite phases' stresses are measured before unloading and after loading again to study the strain path's influence.

By means of this work it is confirmed that the elastic strain path has no influence on the unloading–loading of this TRIP steel. These results prove that conventional loading–unloading cyclic testing is a valid methodology for a detailed characterisation of the elastic modulus and reliable numerical modelling of springback.

1. Introduction and motivation

In the last years, and mainly due to the constantly increasing market competitiveness, there has been a trend towards design free and lightweight structures, leading to the use of more complex geometries and new materials. Advanced high strength steels (AHSS) are taking acceptance in the market due to their good mechanical properties to weight ratio [1]. Among these, TRIP steels present a good drawability associated with a high resistance; their good mechanical properties are due to the presence of residual austenite that can transform into martensite when a stress is applied. This is responsible for hardening of the steel. However, migration from common mild steel to AHSS induces a huge increase in the elastic recovery after forming (springback phenomenon), which is a significant issue for industrial part and die producers [2].

Springback phenomenon carries significant differences between numerical and experimental results [3]. These differences involve an increase of the production costs due to the try-error procedure that has to be used to set up the process. Therefore, a good characterisation of the material becomes crucial to improve springback numerical predictions and to optimise the design of components and the stamping process.

TRIP 700 steel behaviour has already been characterised at different temperatures [4], strain rates [5] and triaxiality states [6], focussing on the plastic behaviour, e.g. yield stress and hardening curve. The elastic behaviour also needs to be defined with a high accuracy in springback simulations [7–14]. Additionally, several authors have stated the non-linear elastic behaviour of some AHSS materials, which implies more complex characterisations as loading–unloading cycles or pre-strained tensile tests [8,9,15–18]. From previous works on TRIP 700 steels [5,19–21] it is concluded that the elastic part of the stress–strain curve during unloading is not a straight line but its curvature evolves with plastic strain. Some authors concluded that the decrease of the elastic modulus is due to microplastic strains while others stated that the second order elasticity is responsible for this variation. At a lower scale, microscopic characterisations focus mainly on the phase transformation mechanisms. These works go from the TRIP effect characterisation [21–25] up to the micro–macro TRIP behaviour modelling [26,27], where microscopic models are homogenised in order to develop a macroscopic behaviour law, through phase percentage evolution [28–31] and micro-residual stress analysis [32] among others.

Cyclic test using loading and unloading at some equivalent strains is a suitable test to characterise the inelastic behaviour of these steels [33]. However, to our knowledge, the influence of the strain path on the inelastic behaviour has not been studied yet. This is essential since the metal strip or the blank suffers different loading and unloading steps when being formed using conventional metal forming techniques, i.e. multi-step deep drawing, roll forming, etc.

Therefore, this paper deals with the strain path's influence on the elastic behaviour of the TRIP 700 steel in order to validate the cyclic testing method for the characterisation of the inelastic behaviour of the AHSS. The cyclic testing method is developed at macroscopic scale, but during a loading cycle, the microstructure evolves as austenite transforms into martensite and it can induce a load transfer between phases [3]. Therefore, in this work the influence of the strain path is analysed at both macroscopic and crystallographic phase's levels. First, the different macroscopic cyclic tests are presented, where the strain path is changed from test to test. In the second part, the macro- and micro-measuring methods are explained. Large deformation strain gages have been used to compare the inelastic behaviour of the specimens at macro-level. In-situ stress measurements have been carried out for different cyclic testing using XRD technique for the micro-analysis. Ferrite and austenite phases' stresses have been measured at different points of the loading–unloading cycles. Finally, experimental results and conclusions are pointed out.

2. Experimental procedures

2.1. Material

The analysed material is a cold-rolled TRIP 700 steel with thickness of 1.5 mm. The chemical composition obtained by optical emission spectroscopy of the steel is shown in Table 1.

At the as-received state, it is a multi-phased steel: it contains ferrite, bainite and about 6%–7% of residual austenite [20].

2.2. Macro-measurements

The loading–unloading cycling test is used classically to analyse the mechanical behaviour of materials during elastic recovery. The test consists in loading the tensile specimen up to a defined specific strain, called hereafter pre-strain, and unloading it after each pre-strain until the relaxed state is achieved (zero stress). Once the first loading–unloading cycle is performed, the specimen is reloaded again up to the next pre-strain and subsequently unloaded. This procedure is repeated until the last cycle is performed.

Three different experiments have been performed. In the first test, called hereafter "baseline test" and mostly used in literature, eight loading–unloading cycles have been carried out: the stress–strain curve evolution has been measured during the whole test. In the second variant, only two loading–unloading cycles have been performed: the final maximum strain is the same as in the baseline test. The results of the second variant test are compared with the baseline test and the influence of previous unloading–loading cycles on the elastic behaviour is analysed. Finally, in the third variant, eight loading–unloading cycles have been performed, like in the baseline test, but unloading has been limited to 80 MPa. By comparing the third variant with the baseline test, the influence of a partial unloading on the evolution of the elastic behaviour is analysed. The different tests are shown in Fig. 1. The different test conditions are summarised in Table 3.

Cycling tests have been performed using specimens according to EN 10 002-1 standard. Samples have been cut using a Robofil 100 wire electrical discharge machine, the rolling direction being parallel to the tensile direction. Experimental tests have been carried out in a 5t Instron-Zwick/Roell universal machine and at $10^{-3}\,s^{-1}$ strain rate.

Table 1
Chemical composition (wt%–iron balance) of the analysed TRIP 700 steel.

C	Si	Mn	P	S	Cr	Ni	Mo	Al	Cu
0.22	0.29	1.82	0.012	0.002	0.03	0.02	0.04	0.86	0.03

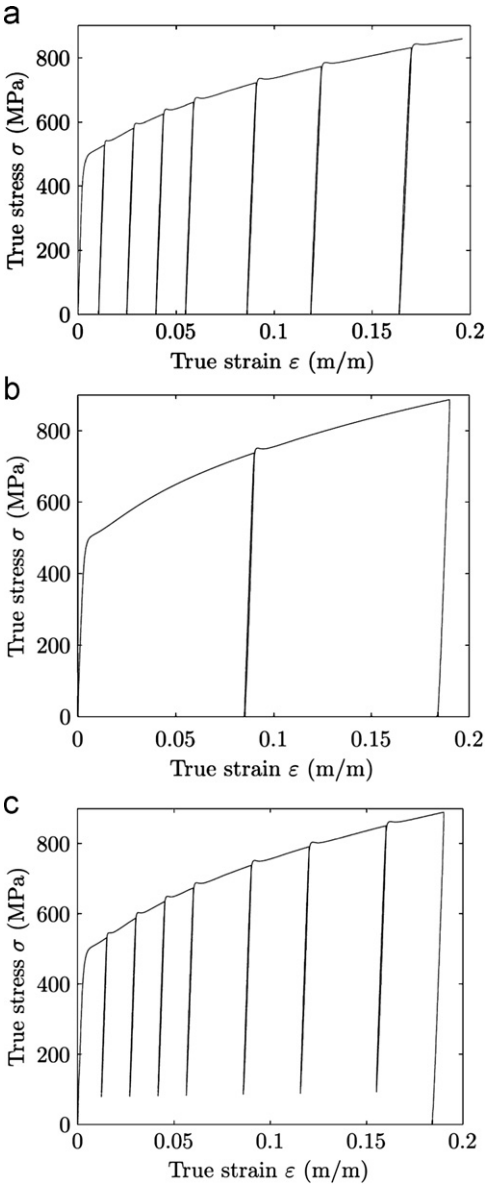

Fig. 1. Results for selected cycling tests: (a) baseline test; (b) second variant and (c) third variant tests.

In order to measure experimental strain with accuracy, Vishay EP-08-250BF-350 large deformation gages have been glued to the specimens. Experimental set-up is shown Fig. 2(a).

2.3. In situ X-ray diffraction micro-measurements

In order to evaluate stress evolution in each phase, in-situ stress measurements using a tensile micromachine have been performed. In Fig. 2(b) the X-Ray diffraction system equipped with the in-situ tensile test device is shown. The tensile specimens' dimensions are $24 \times 4 \times 1.5\ mm^3$; the macroscopic stress and strain have been calculated from force and displacement sensors directly attached to the tensile machine.

X-ray diffraction is often used as it enables a non-destructive evaluation of surface stresses in crystalline materials. Due to the weak penetration depth of X-rays in the matter, only a few micrometres are concerned with the analysis. From the Bragg's

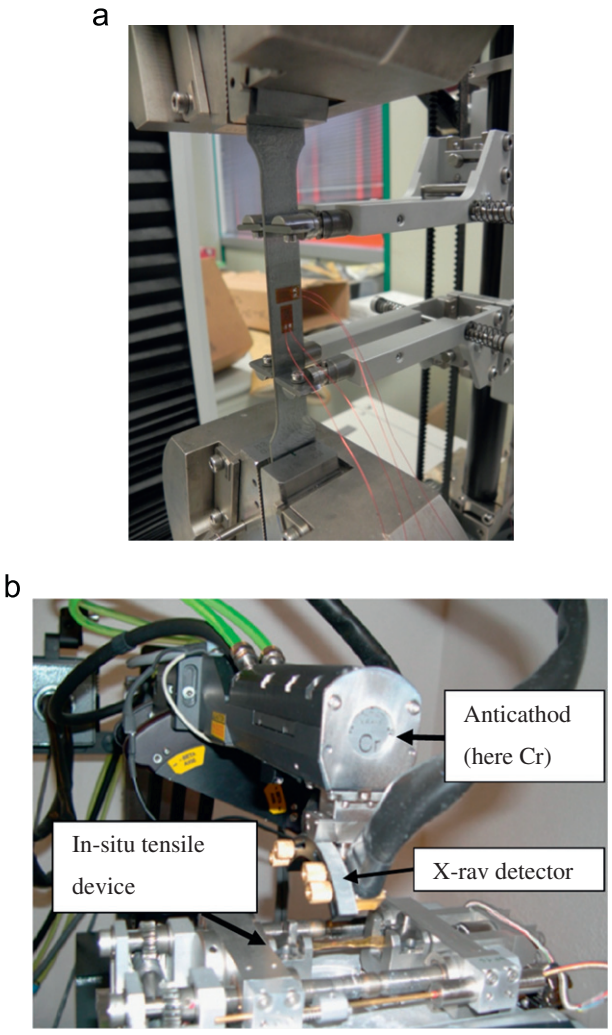

Fig. 2. Experimental set-ups (a) macro-measurements and (b) in-situ micro-measurements.

law, the diffraction angles, $\theta_{hkl,}$ are related to interplanar spacings d_{hkl} of a (hkl) family plane:

$$\lambda = 2d_{hkl}\sin(\theta_{hkl}) \quad (1)$$

In a stress-free material, the interplanar spacings, d_0, do not depend on the planes orientation. If a tensile stress is applied, due to elastic deformation, the interplanar spacings increase for planes perpendicular to the tensile direction and decrease if planes are parallel to the tensile direction. Therefore lattice spacings can be used as an internal strain gauge in the material. Considering Eq. (1), a d_{hkl} variation will induce a shift of the diffraction peak. From the peak shift measurement, the elastic strain is calculated following:

$$\varepsilon_{hkl} = \frac{d_{hkl} - d_0}{d_0} \quad (2)$$

where d_0 is the stress-free value of the interplanar spacing and d_{hkl}, the interplanar spacings under the applied stress. Then the stress value, σ_ϕ, is deduced from Hooke's law, the so-called $\sin^2\psi$ law [35]:

$$\varepsilon_{\phi,\psi} = \frac{1}{2}S_2\sigma_\phi \sin^2\psi + S_1(\sigma_{11}+\sigma_{22}) \quad (3)$$

where S_1 and S_2 are the X-ray elastic constants which depend on the diffracting planes and the material. ϕ and ψ are the reference angles: ϕ states for the measurement direction and ψ is the tilt angle of the specimen with respect to X-ray beam. In isotropic materials, the curve $\varepsilon_{\phi,\psi} = f(\sin^2\psi)$ is a straight line whose slope is proportional to the stress value. In this method, measurements are performed on only one selected (hkl) planes family: the higher the diffraction angle, the better the accuracy. So in multi-phase materials, acquiring conditions differ from one phase to another. As given in the standard NF-EN 15305, austenite stress measurements must be performed on {311} crystallographic planes using Mn Kα radiation and on {211} crystallographic planes using Cr Kα radiation for the ferrite phase. As pro-eutecoid ferrite, ferrite in the bainite and martensite have almost the same crystallographic structure, they diffract at the same angle: it is not possible to separate their contribution. Therefore, in the following, the ferrite stress represents the mean value over these phases.

As in macroscopic tests, stress analysis has been performed at different loading and unloading points using the iXRD stress measurement system from PROTO (Fig. 2b); the collimator diameter was 1 mm; 18 ψ-angles were used with a counting time of 30 s by step. Calibration and alignment were performed with a stress-free powder and a pre-stressed sample. As both phases cannot be analysed with the same radiation the following procedure has been used:

1. Loading of the specimen.
2. Measurement in the ferrite phase using the Cr-radiation.
3. Set up of the Mn radiation.
4. Measurement in the austenite phase.
5. Back to point 1.

Diffraction peaks were fitted using a Gaussian functions. The used X-ray elastic constants are summarised Tables 2 and 3. Error bars were estimated from the difference between the measured data and the regression result: it represents the standard deviation calculated with least squares residue. Moreover, each test has been repeated three times to estimate the repeatability.

That way, the macroscopic loading (given by the force sensor) and the local stress in each phase have been obtained. Comparing stresses before unloading and after loading the influence of cycling and the strain path can be analysed from a microscopic point of view [29,31,34].

3. Experimental results

3.1. Macro-results

3.1.1. Young's modulus evolution

Baseline test has been used to calculate Young's modulus for each loading test at a given strain. Linear regression technique following the E111-97 standard "Standard Test Method for Young's Modulus, Tangent Modulus, and Chord Modulus" has been used for calculation, taking 100 MPa and 350 MPa as lower and upper limits, respectively. Three specimens have been tested; the averaged moduli on the three measurements are presented. Young's modulus decreases with the true strain as it can be seen Fig. 3; it is about 196 GPa at the initial state and decreases to

Table 2
X-ray elastic constants.

	$1/2S_2$ (10^{-6} MPa^{-1})	$-S_1$ (10^{-6} MPa^{-1})
Austenite	7.18	1.20
Ferrite	5.92	1.28

Table 3
Loading–unloading cycling tests. Pre-strain values and unloading types.

Test id	Pre-strain								Unloading type
Baseline	0.015	0.03	0.045	0.06	0.09	0.12	0.16	0.19	relaxation
2nd variant	–	–	–	–	0.09	–	–	0.19	relaxation
3rd variant	0.015	0.03	0.045	0.06	0.09	0.12	0.16	0.19	80 MPa
Micro-cyclic	–	–	0.04	0.06	–	–	–	–	relaxation

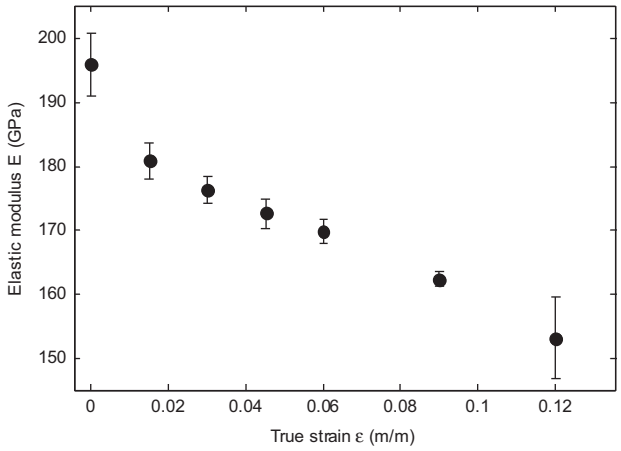

Fig. 3. Loading elastic modulus at different pre-strains.

155 GPa after 12% strain. The maximum difference is about 21%, which can strongly affect numerical predictions.

3.1.2. Macro-strain path influence analysis

The baseline test has been compared with second and third variants in order to study the influence of the strain path on the recovery behaviour of the material. The elastic unloading–loading behaviours after 9% and 19% of pre-strain have been analysed for each test and compared.

Fig. 4 shows the comparison between the baseline test and the second variant (fewer cycles) at 9% pre-strain. At the macroscopic level, no difference is observed between both paths. Therefore, it could be said that there is no influence on performing intermediate unloading–loading. Similar results are obtained for 19% of pre-strain and are not plotted. The differences between both elastic unloading–loading paths do not exceed 2%.

Third variant and baseline tests have been compared to analyse the effect of a partial unloading. Fig. 5 represents the comparison between the elastic unloading–loading of the baseline test and third variant test. For the last one the imposed strain is 9% and the samples were unloaded down to 80 MPa. Like in previous comparison, both unloading behaviours do not differ by more than 2%, obviously for the loading they differ due to different unloading limits. Similar results are obtained for 19% of pre-strain but are not plotted in this paper.

3.2. X-ray diffraction results

No clear differences have been observed by comparing the three macro-tests. As the steel is a multi-phase steel, i.e. with different mechanical properties, it has also been studied the elastic behaviour of the individual phases during a baseline test; in-situ tensile tests combined with X-ray diffraction as presented previously have been used.

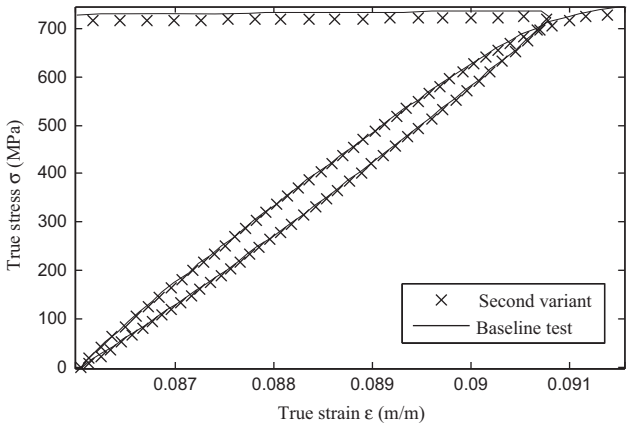

Fig. 4. Comparison between the unloading step after 9% of pre-strain of the baseline and second variant tests.

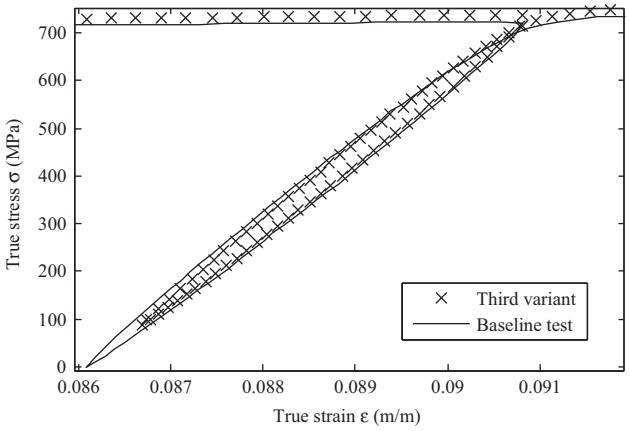

Fig. 5. Comparison between the elastic unloading–loading after 9% of pre-strain of the baseline and third variant tests.

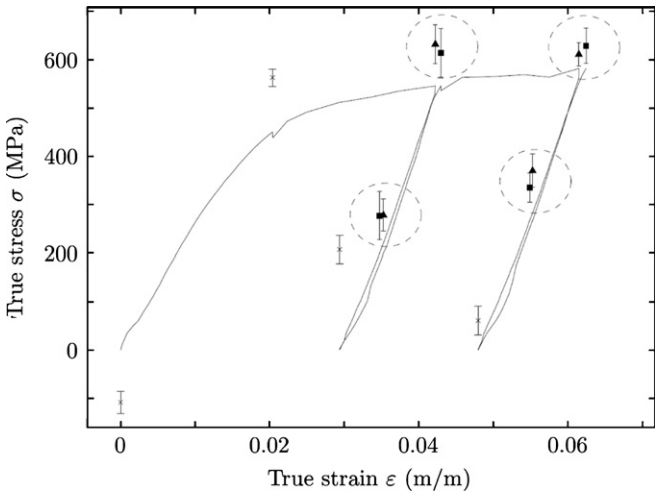

Fig. 6. Evolution of austenite stress during the in-situ tensile test.

3.2.1. Stress analysis in austenite

Fig. 6 shows the results in the austenite phase: austenite stress values are indicated by dots. The macroscopic stress–strain curve is plotted in solid line. Measurements performed at the same macroscopic stress during loading and unloading are rounded by dashed circles: square dots stand for loading and triangle dots for unloading. It has to be pointed out that this is a surface measurement.

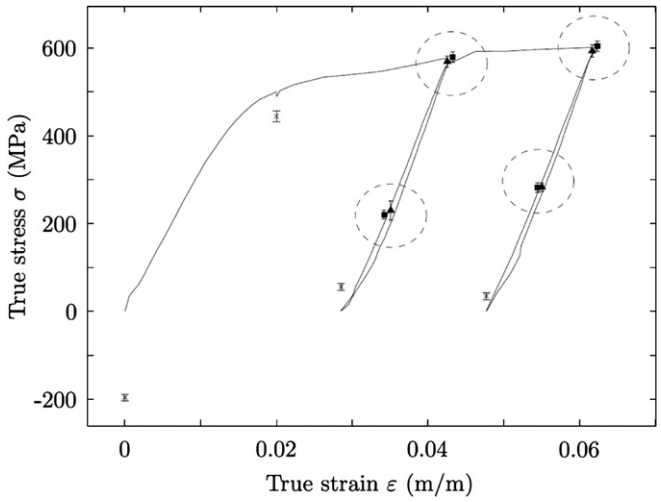

Fig. 7. Evolution of the ferrite stress during the in-situ tensile test.

At the initial state, the austenite stress is negative, i.e. austenite is in compression at the surface. This can be due to surface preparation [37] and the skin-pass step performed on the sheet. Then it is noticed that the austenite phase is always in tension during the tensile test. The austenite stress is higher than the macroscopic one; the difference varies between 50 MPa and 70 MPa. This means that austenite is harder than the other phases. Phase rigidity is assumed to be the reason for this effect. If similar measurements are compared during loading and unloading, the difference between the austenite stress states remains lower than the measurement uncertainty. Thus, austenite stress state does not seem to be affected by the strain paths.

3.2.2. Stress analysis in ferrite

At each loading points, a stress analysis has also been performed in the ferrite phase. As mentioned previously, in fact, this is a mean value over ferrite and martensite phases. Results are shown Fig. 7. Dots represent ferrite stress; the macroscopic stress–strain curve is plotted in solid line. Measurements performed at the same macroscopic stress during loading and unloading are rounded by dashed circles: square dots stand for loading and triangle dots for unloading.

At the initial state the ferrite is in compression: its stress value is around $-200\,\text{MPa} \pm 8\,\text{MPa}$. Both phases, ferrite and austenite, are in compression at the initial state whereas no macroscopic stress is applied. This is a surface measurement; as previously mentioned, this phenomenon could be due to the sample polishing and the skin-pass procedure performed on the sheet.

The ferrite stress values are lower than the macroscopic stress values for low strains, around 50 MPa at the yield stress, and seem to converge to the macroscopic stress in larger strains than 3%–4%. The microstructure of TRIP steels is retained austenite embedded in a primary matrix of ferrite. In addition to a minimum of 5 vol% of retained austenite, hard phases such as martensite and bainite are present in varying amounts. When the plastic strain increases the TRIP transformation occurs and the percentage of residual austenite decreases. The stress addition theory [33,36] states that the stress value supported by each phase depends on its volume fraction,

$$\sigma_{\text{macro}} = \sum \sigma_i V_i \tag{4}$$

where σ_i is the stress of the i-th phase with V_i volume fraction. Therefore, as low percentage of residual austenite is expected at high strains, the microscopic-stress value of ferrite should converge with the macroscopic stress-value.

Comparing the micro-measurements before and after unloading cycle it can be noted that the unloading–loading cycle has not changed the ferrite stress value.

4. Conclusions

In this work the strain path's influence on the elastic behaviour of the TRIP 700 steel has been analysed at macroscopic and microscopic levels. The following conclusions could be obtained:

- The elastic modulus decreases strongly when the pre-strain increases. A decrease of about 20% is observed at 12% of pre-strain. This confirms that proper characterisation of material is crucial for reliable numerical modelling of springback.
- No clear differences have been found when changing the elastic strain path at macroscopic level (first three variants). From the comparison of the second variant and the baseline tests, it can be concluded that the number of elastic unloading–loading cycles performed before an unloading phase is not relevant for the elastic unloading behaviour. In the same way, by comparing the third variant and the baseline tests, the unloading limit stress does not seem to affect the elastic unloading behaviour. Therefore, elastic behaviour does not depend on the strain path for the selected steel and conditions.
- Micro-stress states before and after the elastic unloading–loading cycles are similar (taking into account the measurement uncertainty) during the X-ray diffraction measurements. Therefore, no influence of the elastic strain path is shown at microscopic level.

By means of this work it has been confirmed that the elastic strain path does not seem to influence the unloading–loading behaviour of the TRIP steel. Therefore conventional cyclic testing (baseline test in this paper) is an appropriate methodology for a detailed characterisation of the elastic modulus and reliable numerical modelling of springback.

Acknowledgement

The work presented in this paper has been carried out with the financial support of the Department of Education, Universities and Research of the Basque Government.

References

[1] W.J. Dan, S.H. Li, W.G. Zhang, Z.Q. Lin, Mater. Des. 29 (3) (2008) 604–612.
[2] Zhang L., Shi M.F., Issues Concerning Material Constitutive Laws and Parameters in Springback Simulations. SAE 0.1:1002, 1999.
[3] A. Asgari, M. Pereira, B. Clark, M. Dingle, P. Hodgson, AIP Conf. Proc. 712 (2004) 977.
[4] E. Doege, S. Kulp, C. Sunderkotter, Steel Res. 73 (2002) 303–308.
[5] D. Pitchure, R. Ricker, J. Mater. Eng. Perform. 16 (2007) 349–353.
[6] H. Huh, S. Kim, J. Song, J. Lim, Int. J. Mech. Sci. 50 (2008) 918–931.
[7] S. Chatti, Comp. Struct. 88 (2010) 769–805.
[8] S. Chatti, N. Hermi, Comp. Struct. 89 (2011) 1367–1377.
[9] R. Cleveland, A. Ghosh, Int. J. Plasticity 18 (2002) 769–785.
[10] J. Gelin, S. Thibaud, N. Boudeau, AIP Conf. Proc. 778 (2005) 101–106.
[11] M. Halilovic, M. Vrh, B. Stok, AIP Conf. Proc. 908 (2007) 925–930.
[12] F. Morestin, M. Boivin, Nucl. Eng. Design 162 (1996) 107–116.
[13] T. Shan, L. Liu, Adv. Mater. Res. 221 (2011) 152–158.
[14] M. Vrh, M. Halilovic, B. Stok, J. Mech. Eng. 54 (2008) 288–296.
[15] S. Asgari, M. Pereira, B. Rolfe, M. Dingle, P. Hodgson, J. Mater. Process. Technol. 203 (2008) 129–136.
[16] P.A. Eggertsen, K. Mattiasson, Int. J. Mater. Forming 4 (2011) 103–120.
[17] T. Hama, H. Takuda, Int. J. Plasticity 27 (2011) 1072–1092.
[18] L. Sun, R. Wagoner, Int. J. Plasticity 27 (2011) 1126–1144.

[19] Fei, D., Hodgson, P., (2006) Experimental and Numerical Studies of Springback in Air V-Bending Process for Cold Rolled Trip Steels, Nuclear Engineering and Design 236, 1847–1851.
[20] R. Perez, J. Benito, J. Prado, ISIJ Int. 45 (2005) 1925–1933.
[21] H.Y. Yu, Mater. Design 30 (2009) 846–850.
[22] T. Bhattacharyya, S.B. Singh, S. Das, A. Haldar, D. Bhattacharjee, Mater. Sci. Eng. A 528 (2011) 2394–2400.
[23] A. Weidner, A. Glage, H. Biermann, Procedia. Eng. 2 (2010) 1961–1971.
[24] J. Serri, M. Cherkaoui, J. Eng. Mater. Technol. 130 (2008) 31009–31010.
[25] N. Boudeau, S. Thibaud, J. Gelin, J. Mater. Process. Technol. 177 (2006) 433–438.
[26] L. Li, S. Tikun, Adv. Mater. Res. 221 (2011) 405–410.
[27] S. Asgari, P. Hodgson, C. Yang, B. Rolfe, Comput. Mater. Sci. 45 (2009) 860–866.
[28] T. Gnaupel-Herold, A. Creuziger, Mater. Sci. Eng. A 528 (2011) 3594–3600.
[29] S. Berveiller, K. Inal, R. Kubler, A. Eberhardt, E. Patoor, J. Phys. IV (Proceedings) 115 (2004) 261–268.
[30] S. Brauser, A. Kromm, T. Kannengiesser, M. Rethmeier, Scripta Mater. 63 (2010) 1149–1152.
[31] A. Weidner, A. Glage, H. Biermann, Procedia. Eng. 2 (2010) 1961–1971.
[32] K. Choi, W. Liu, X. Sun, M. Khaleel, Acta Mater. 57 (2009) 2592–2604.
[33] P.A. Eggertsen, K. Mattiasson, Int. J. Mech. Sci. 51 (2009) 547–563.
[34] C.F. Jatczak, Retained Austenite and its Measurement by X-ray Diffraction, SAE Preprints, 1980.
[35] V. Hauk, Structural and Residual Stress Analysis by Non-destructive Methods, Elsevier, Amsterdam, 1997.
[36] V. Kouznetsova, M. Geers, Mech. Mater. 40 (2008) 641–657.
[37] M.R. Berrahmoune, S. Berveiller, K. Inal, A. Moulin, E. Patoor, Mater. Sci. Eng. A 378 (2004) 304–307.